Do we live in a "small Universe"?

Ralf Aurich[1], **Holger S. Janzer**[1], **Sven Lustig**[1], **and Frank Steiner**[1]

[1]Institut für Theoretische Physik, Universität Ulm,
Albert-Einstein-Allee 11, D-89069 Ulm, Germany

Abstract. We compute the effects of a compact flat universe on the angular correlation function, the angular power spectrum, the circles-in-the-sky signature, and the covariance matrix of the spherical harmonics coefficients of the cosmic microwave background radiation using the full Boltzmann physics. Our analysis shows that the Wilkinson Microwave Anisotropy Probe (WMAP) three-year data are well compatible with the possibility that we live in a flat 3-torus with volume $\simeq 5 \cdot 10^3 \mathrm{Gpc}^3$.

PACS numbers: 98.80.-k, 98.70.Vc, 98.80.Es

1. Introduction

At present, all data are consistent with, and in fact strongly support, the standard big bang model based on general relativity and the cosmological principle leading to the general class of Friedmann-Lemaître universes possessing the space-time structure $R \times M^3$. Here R describes cosmic time and M^3 the three-dimensional comoving spatial section of constant curvature $K = 0$ or $K = \pm 1$. Since the Einstein gravitational field equations are differential equations, they govern the local properties of space-time but not the global geometry of the Universe at large, i. e. they do not determine the spatial curvature and topology, and thus the shape of the Universe.

Although a full quantum theory of gravity has not yet been established, it is commonly assumed that our Universe emerged from quantum fluctuations during the Planck era and that its spatial curvature and topology are invariants, i. e. have not changed ever since. The spatial curvature K can be inferred from astronomical observations of the total energy density ϵ_{tot} of the Universe (at the present epoch) which is usually expressed in terms of the dimensionless density parameter $\Omega_{\mathrm{tot}} = \epsilon_{\mathrm{tot}}/\epsilon_{\mathrm{crit}}$. ($K = 0$ for $\Omega_{\mathrm{tot}} = 1$, $K = \pm 1$ for $\Omega_{\mathrm{tot}} \gtrless 1$. $\epsilon_{\mathrm{crit}} = 3H_0^2 c^2/(8\pi G)$, where $H_0 = 100h(\mathrm{km/s})/\mathrm{Mpc}$ denotes the Hubble constant.)

Measurements of the temperature anisotropy of the cosmic microwave background (CMB) by NASA's satellite Wilkinson Microwave Anisotropy Probe (WMAP) suggest (using the 3-year data combined with other observations) $\Omega_{\mathrm{tot}} \simeq 1.0$ [1]. Since this value for the density parameter is compatible with Euclidean geometry, we shall assume in this paper that our Universe is, indeed, flat. (For a discussion of positively or negatively

curved universes, see e. g. [2, 3, 4] and [5, 6, 7], respectively.) Having thus fixed the curvature, there remains the question of the topology of our Universe.

It is a mathematical fact that fixing the curvature K does not determine uniquely the topology and thus the shape of the universe. Only if it is *assumed* that the spatial section is simply connected, it follows that the topology is (in the flat case) given by the infinite Euclidean 3-space E^3. Exactly this assumption is made in the popular ΛCDM model [1] which is composed of radiation (r), ordinary baryonic matter (b), cold dark matter (cdm) and has a cosmological constant Λ, i. e. $\Omega_{\rm tot} = \Omega_{\rm r} + \Omega_{\rm b} + \Omega_{\rm cdm} + \Omega_\Lambda \equiv 1$.

It is the purpose of this paper to demonstrate that the WMAP 3yr data [1] are well compatible with the possibility that we live in a "small Universe" having the shape of a flat 3-torus whose fundamental domain is a cube with side length $L \simeq 4$ corresponding to a volume of $\simeq 5 \cdot 10^3 {\rm Gpc}^3$. ($L$ is given in units of the Hubble length $L_{\rm H} = c/H_0 \simeq 4.26{\rm Gpc}$ for $h = 0.704$.) For previous works on a toroidal universe, see [8, 9, 10, 11, 12, 13, 14, 15, 16, 17, 18, 19, 20, 21, 22, 23, 24, 25, 26, 27]. It turns out that the torus model describes the data much better than the best-fit ΛCDM model since it exhibits the suppression of the CMB anisotropy at large scales first observed by COBE [28].

Let us point out that Linde [29] has argued recently that a compact flat universe like the toroidal universe provides the simplest way to solve the problem of initial conditions for the low-scale inflation. While the quantum creation of a closed or an infinite open inflationary universe is exponentially suppressed, there is no such suppression for the toroidal universe.

In [1] the WMAP team offers several sets of cosmological parameters depending on which cosmological data sets are taken into account. In this paper we use the cosmological parameters of the ΛCDM model of Table 2 in [1] based on all astronomical observations, see their column "3 Year + ALL Mean", i. e. $\Omega_{\rm b} = 0.044$, $\Omega_{\rm cdm} = 0.223$, $\Omega_\Lambda = 0.733$, $h = 0.704$, $n_s = 0.947$, $\tau = 0.073$. The distance to the surface of last scattering (SLS) is $L_{\rm SLS} = \Delta\eta L_{\rm H} \simeq 14.2{\rm Gpc}$ where $\Delta\eta = \eta_0 - \eta_{\rm SLS} = 3.329$ (η is the conformal time).

The temperature fluctuations $\delta T(\hat{n})$ of the CMB are calculated using the full Boltzmann physics of the coupled baryon-photon fluid, i. e. the ordinary and the integrated Sachs-Wolfe effect, the Doppler contribution, the Silk damping and the reionization are taken into consideration. The reionization is taken into account by modifying the ionization fraction x_e computed with recfast [30]

$$x_e = x_e^{\rm recfast} + \left\{1 + \frac{Y_p}{2Y_p(1-Y_p)}\right\} \frac{{\rm erfc}(\alpha(z-\beta))}{2} \qquad (1)$$

by adding a term proportional to an erfc-function with parameters α and β. (Here $Y_p = 0.24$ denotes the Helium abundance.) We set $\alpha = 0.4$ and $\beta = 9$ which leads to an optical depth of $\tau = 0.073$.

The crucial difference between the toroidal and the simply connected ΛCDM model arises from the discrete spectrum of the vibrational modes $\{\vec{k} = \frac{2\pi}{L}\vec{\nu}; \vec{\nu} = (\nu_x, \nu_y, \nu_z) \in \mathbb{Z}^3\}$ due to the periodic boundary conditions imposed on the regular

solutions of the Helmholtz wave equation for the 3-torus. (Note that a given wave number $k = |\vec{k}|$ contributes with a highly irregular multiplicity determined by the number of representations of $a \in \mathbb{N}$ by a sum of 3 squares of integers.) Since the 3-torus does not support wave lengths longer than L, there is an infrared cutoff $k \geq 2\pi/L$ (the mode $k = 0$ is not included being a pure gauge mode) which leads to the observed suppression of CMB power at large scales as we shall show now. In our calculations we use the exact mode spectrum for the first 10 000 eigenvalues, i. e. the first 5 503 602 eigenmodes. The contribution of the higher modes is taken into account by a smooth remainder term as in the case of an infinite universe.

2. Large scale temperature correlations and the angular power spectrum

Let us consider the two-point temperature correlation function $C(\vartheta) = \langle \delta T(\hat{n})\, \delta T(\hat{n}') \rangle$, $\hat{n} \cdot \hat{n}' = \cos\vartheta$, where $\langle \ldots \rangle$ denotes an ensemble average over the primordial fluctuations, respectively, an ensemble average over the universal observers. In Fig. 1 we show as a function of the torus length L the integrated weighted temperature correlation difference

$$I := \int_{-1}^{1} d(\cos\vartheta) \frac{(C^{\mathrm{model}}(\vartheta) - C^{\mathrm{obs}}(\vartheta))^2}{\mathrm{Var}(C^{\mathrm{model}}(\vartheta))} \tag{2}$$

between $C^{\mathrm{model}}(\vartheta)$ for the torus model and $C^{\mathrm{obs}}(\vartheta)$ for four data sets derived from the WMAP 3yr data. The full and the dotted curves show $I(L)$ derived from the ILC 3yr map and the TOH 3yr cleaned map [31] both with Kp0 mask, respectively, while the dashed and dotted-dashed curves refer to the ILC 3yr map and the TOH 3yr cleaned map both without mask. The horizontal lines show the corresponding results for the best-fit infinite ΛCDM model. It is seen from Fig. 1 that $I(L)$ possesses a pronounced minimum at $L = 3.86$ for the maps with Kp0 mask, respectively at $L = 4.35$ for the maps without mask, which allows us to fix the best-fit torus model depending on the used data set. This shows that the WMAP-ILC 3yr map and the TOH 3yr cleaned map lead to the same best torus model. The uncertainty results mainly from the data near the galactic plane, i. e. by including them using no mask or by excluding them by applying the Kp0 mask. However, in both cases, the torus length L is close to $L = 4$, such that the main result is not affected by the foregrounds near the galactic plane. The values of $I(L)$ obtained for the best-fit models are substantially lower than the corresponding values for the best-fit ΛCDM model demonstrating the suppressed CMB power of the toroidal universe. Obviously, if the toroidal universe gets too large ($L \gtrsim 9$), the results are very similar to the infinite flat universe.

In Fig. 2 we show the mean temperature correlation function $C(\vartheta)$ for the torus model with the length $L = 3.86$ (full line) together with the 1σ standard deviation (grey band). The 1σ band is obtained from 10 000 sky map simulations of the considered torus model. For each realization the correlation function $C(\vartheta)$ is computed which in turn gives the standard deviation for this sample. This is compared to the WMAP-ILC 3yr (Kp0) data (dotted line) and the best-fit ΛCDM model (dashed line). As expected, the torus model is in much better agreement with the data than the ΛCDM model. Notice

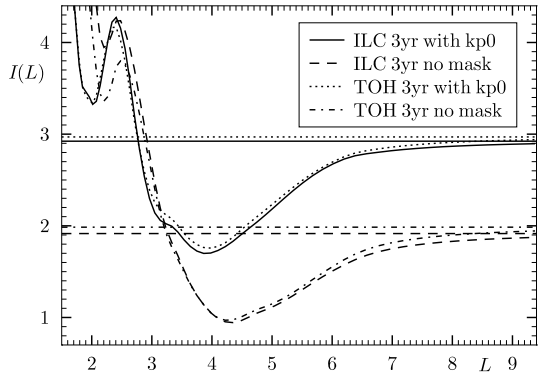

Figure 1. The integrated weighted temperature correlation difference $I(L)$ is shown for the torus model in dependence on the length L and for the best-fit ΛCDM model (straight horizontal lines) as described in [1] incorporating the cosmological parameters of the "WMAP3yr + ALL" model. The models are compared with four data sets derived from the WMAP 3yr data.

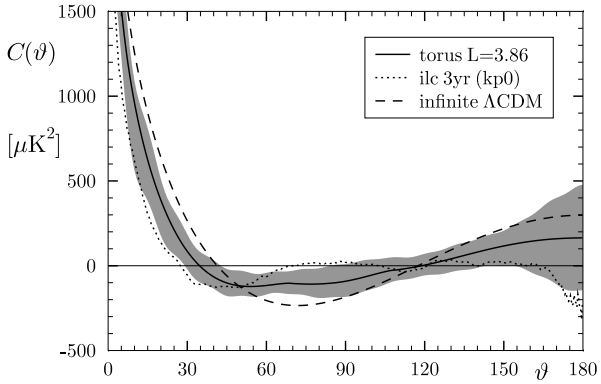

Figure 2. The temperature correlation function $C(\vartheta)$ is shown for the torus model with the length $L = 3.86$ and for the best-fit ΛCDM model. The grey band shows the 1σ deviation computed from 10 000 simulations of the $L = 3.86$ torus model.

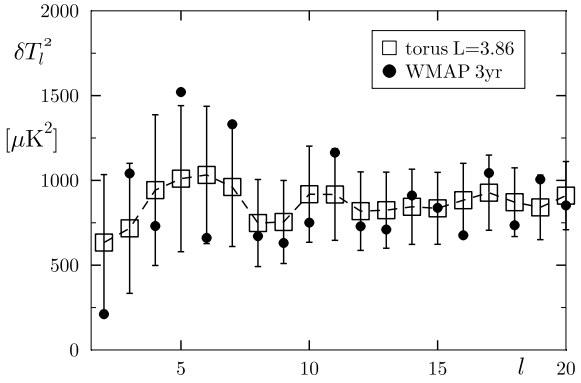

Figure 3. The angular power spectrum δT_l^2 is shown for the torus model with the length $L = 3.86$ with the cosmic variance in comparison with the WMAP 3yr data.

that the difference $C^{\rm obs}(\vartheta) - C^{\rm model}(\vartheta)$ between the data and the torus model is almost always a factor two smaller than the difference between the data and the ΛCDM model. In Fig. 3 we compare the power spectrum $\delta T_l^2 = l(l+1)C_l/(2\pi)$ (including cosmic

variance) for the same torus model with the WMAP 3yr power spectrum [1], which is produced by combining the maximum likelihood estimated spectrum from $l = 2 - 10$ with the pseudo-C_l based cross-power spectra for $l > 10$. This WMAP 3yr power spectrum matches the power obtained from the previous sky maps without using any masks. Since we are mainly concerned with the large scale structure, we present only the low multipoles with $2 \leq l \leq 20$. We have checked, however, that the power spectrum reproduces correctly the higher acoustic peak structure. The overall normalization is the only free parameter and has been determined by adjusting the power spectrum in the range $20 \leq l \leq 100$ to the WMAP data.

In Fig. 4 and Fig. 5 a similar comparison is carried out for the torus model with $L = 4.35$ which now refers to the WMAP-ILC 3yr data without mask. Again a remarkable agreement with the data is found.

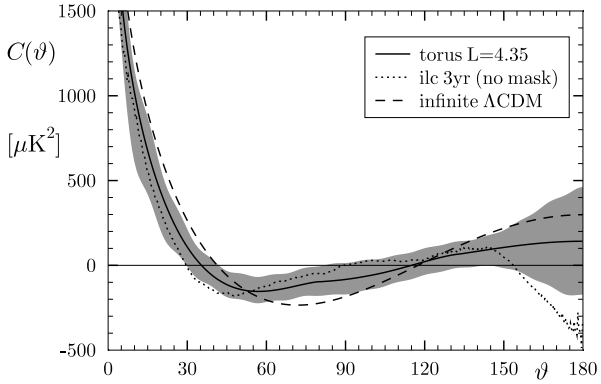

Figure 4. The temperature correlation function $C(\vartheta)$ is shown for the torus model with the length $L = 4.35$ and for the best-fit ΛCDM model. The grey band shows the 1σ deviation computed from 10 000 simulations of the $L = 4.35$ torus model.

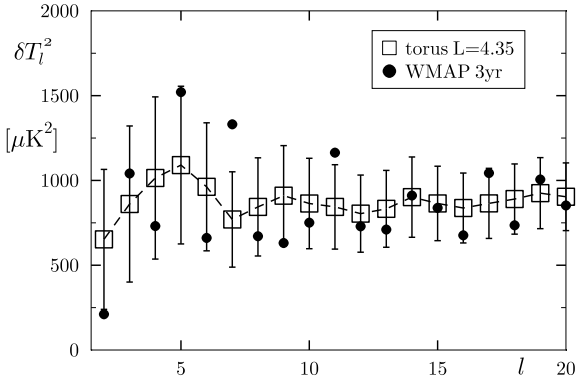

Figure 5. The angular power spectrum δT_l^2 is shown for the torus model with the length $L = 4.35$ with the cosmic variance in comparison with the WMAP 3yr data.

3. The circles-in-the-sky signature

Up to now we have compared the statistical properties for the CMB of a torus model with the observations. There are, however, two quantities, which can reveal the topology of the Universe more directly. Besides a signature in the covariance matrix, to which we devote the next section, this is the circles-in-the-sky signature [32]. On each circle pair on the CMB sky which is connected by the periodicity condition of the topological cell, there should be similar temperature fluctuations due to the Sachs-Wolfe effect. Expanding the temperature $\delta T_i(\phi)$ along a circle in a Fourier series $\delta T_i(\phi) = \sum_m T_{im} e^{\mathrm{i}m\phi}$, $0 \leq \phi \leq 2\pi$, allows one to define the m-weighted circle signature for two circles i and j having a radius α as [22]

$$S_{ij}(\alpha, \beta) \; := \; \frac{2 \sum_m m T_{im} T^{\star}_{jm} e^{\mathrm{i}m\beta}}{\sum_m m(|T_{im}|^2 + |T_{jm}|^2)} \quad . \tag{3}$$

The angle β takes a possible shift between the two circles into account. In [22] the WMAP 1yr data are analysed and no topological signature is found. In order to investigate the question whether this negative result already rules out a torus cell as advertised in the previous section, we produce sky-map simulations for a torus with length $L = 4$ using the full Boltzmann physics and taking all eigenmodes up to the wavenumber $k = 384.75$ into account, i. e. in total 61,556,892 different wavevectors $\vec{k}$. The contributions of the modes are computed up to $l_{\max} = 1000$. A torus model with $L = 4$ possesses 3 circle pairs with radius $\alpha \simeq 53.08^\circ$ and 6 circle pairs with radius $\alpha \simeq 31.84^\circ$. The sky maps are computed in a HEALPix resolution $N_{\mathrm{side}} = 512$ and are then smoothed to a resolution of 0.5° and finally downgraded to $N_{\mathrm{side}} = 128$. The maximum $S(\alpha) := \max_{ij\beta} S_{ij}(\alpha, \beta)$ of the circle signature (3) reveals the torus cell clearly as shown in Fig. 6, where the arrows indicate the peaks corresponding to the two radii. Now we disturb the sky maps by modifying the spherical expansion coefficients

$$a_{lm} \; \rightarrow \; \frac{1}{\sqrt{1+f^2}} \left(a_{lm} \, + \, f \, a_{l,p(m)} \right) \quad , \tag{4}$$

where f is a constant factor and $p(m)$ is a permutation of $m \in [-l, l]$. With increasing f an increasingly disturbed sky map is generated without altering the statistical properties since only the l subspace is permuted. We found that the topological peaks in the circle signature $S(\alpha)$ vanish if the sky maps are modified by 50μK on the average (see Fig. 6). Thus the crucial question emerges: what is the accuracy of the present CMB sky maps, i. e. is the CMB accuracy better than 50μK? In the latter case the analysis carried out in [22] would rule out the torus model. The ILC map provided by the WMAP team does not specify the accuracy, and its usage for cosmological analyses is not recommended.

Let us at first discuss the detector noise which is given by the WMAP team [33] for the sky maps for the 8 differencing assemblies x with $x \in \{Q_1, Q_2, V_1, V_2, W_1, W_2, W_3, W_4\}$. We construct from the 8 foreground reduced sky maps δT_x a mean value per pixel $\overline{\delta T}(i) := \frac{1}{8} \sum_x \delta T_x(i)$ where i denotes the pixel number with $i \in \{0, 1, .., 12N^2_{\mathrm{side}} - 1\}$. In order to carry out the average, the differencing assemblies

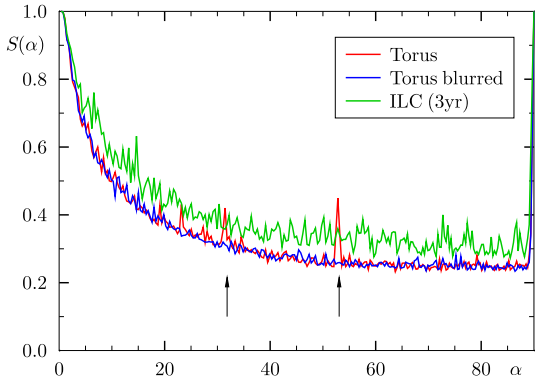

Figure 6. The circles-in-the-sky signature $S(\alpha)$ is shown in dependence on the radius α of the back-to-back circles for a sky-map simulation of a torus with $L = 4$ (red) showing peaks at the corresponding circle radii $\alpha \simeq 31.84°$ and $\alpha \simeq 53.08°$ (indicated by arrows). Disturbing this sky map by 50μK destroys this signature (blue). The result for the ILC-3yr map of the WMAP team is displayed as a green curve which possesses generally larger values than the simulation.

$N_{\rm side}$	128	256	512
$\langle\sigma(i)\rangle^{\rm Kp2}_{\rm 1yr}$	47.3 ± 15.5	64.2 ± 20.8	73.7 ± 24.5
$\langle\sigma(i)\rangle^{\rm Kp2}_{\rm 3yr}$	26.9 ± 8.9	36.9 ± 12.0	42.9 ± 14.5

Table 1. The average scatter (6) of the pixels outside the Kp2 mask is given in μK for the 1yr and the 3yr data with respect to the 8 differencing assemblies. The standard mean deviation of $\sigma(i)$ from $\langle\sigma(i)\rangle^{\rm Kp2}$ is also given.

x are smoothed to the common resolution of the Q_1 band. With this mean value one can define a root mean square deviation per pixel

$$\sigma(i) \;:=\; \sqrt{\frac{\sum_x \left(\delta T_x(i) - \overline{\delta T}(i)\right)^2}{7}} \tag{5}$$

measuring the scatter around the mean value $\overline{\delta T}(i)$ of a pixel. From this root mean square deviation $\sigma(i)$ one can define an average over a given domain which we take as the area outside the Kp2 mask of the 3 year WMAP data excluding also point sources, i. e. we define

$$\langle\sigma(i)\rangle^{\rm Kp2} \;:=\; \frac{\sum_s \sigma(s)}{\sum_s 1} \quad , \tag{6}$$

where the sums run only over the pixels outside the Kp2 mask. The results are presented in Table 1 for three different $N_{\rm side}$ resolutions for the 1yr and the 3yr sky maps. In the case of the highest resolution $N_{\rm side} = 512$ a mean scatter of 74μK and 43μK around the averaged temperature value is obtained for the 1yr and the 3yr maps, respectively.

frequency	$\Delta^{1\mathrm{yr}}_{\mathrm{fore}}$	$\Delta^{3\mathrm{yr}}_{\mathrm{fore}}$	$\Delta^{1\mathrm{yr}}_{3\mathrm{yr}}$
K			34.1
Ka			25.9
Q	66.3	28.9	21.3
V	33.1	6.2	16.7
W	50.5	5.3	22.1

Table 2. The mean amplitude of the foreground which is taken into account in the 1yr and 3yr data outside the Kp2 mask is listed in the 2nd and 3rd column. The mean difference between the 1yr and 3yr data outside the Kp2 mask is given in the last column. The values are given in μK.

Downgrading the maps to lower values of N_{side} averages neighbouring pixels and thus reduces the detector noise. The lowest resolution for which a circle signature $S(\alpha)$ can be computed is $N_{\mathrm{side}} = 128$. Even in this case a mean scatter of 47μK and 27μK is obtained. Since the negative result in [22] with respect to a topological detection is based on the one-year data with a mean scatter of $\langle\sigma(i)\rangle^{\mathrm{Kp2}}_{1\mathrm{yr}} = 47\mu$K outside the Kp2 mask, a possible existing signature can with this accuracy easily be masked as the simulation presented in Fig. 6 demonstrates.

Until now the focus was on the domain outside the Kp2 mask in order to obtain an estimate for the accuracy of the temperature pixel values ignoring a problematic foreground contamination. Within the Kp2 mask which covers 15% of the sky, the foreground dominates the CMB signal and an additional uncertainty with respect to the foreground removal arises. In the cleaned 3yr maps "substantial errors ($\geq 30\mu$K) remain inside the Kp2 cut due to the limitations in the template model" [33]. This residual foreground contamination is also the likely reason why we obtain different favoured lengths L of the torus cell depending on using the Kp0 mask or not as discussed in the previous section. An estimate for the uncertainty in the foreground removal procedure is obtained by taking the difference between the primary maps $\delta T(i)_{\mathrm{pri}}$ and the foreground reduced maps $\delta T(i)_{\mathrm{forered}}$ per frequency band provided by the WMAP team, i. e. by defining the average difference $\Delta^{1\mathrm{yr}}_{\mathrm{fore}} := \langle\delta T(i)^{1\mathrm{yr}}_{\mathrm{pri}} - \delta T(i)^{1\mathrm{yr}}_{\mathrm{forered}}\rangle^{\mathrm{Kp2}}$ and $\Delta^{3\mathrm{yr}}_{\mathrm{fore}} := \langle\delta T(i)^{3\mathrm{yr}}_{\mathrm{pri}} - \delta T(i)^{3\mathrm{yr}}_{\mathrm{forered}}\rangle^{\mathrm{Kp2}}$ outside the Kp2 mask. One obtains from Table 2 large differences in the component which is considered as foreground from the 1yr to the 3yr data. The signal which is considered as foreground is much smaller in the 3yr data than in the 1yr data. This change can be compared with the average difference $\Delta^{1\mathrm{yr}}_{3\mathrm{yr}} := \langle\delta T(i)^{1\mathrm{yr}}_{\mathrm{pri}} - \delta T(i)^{3\mathrm{yr}}_{\mathrm{pri}}\rangle^{\mathrm{Kp2}}$ between the 1yr and 3yr data which is also given in Table 2. An order of magnitude estimate of the foreground uncertainty may thus lie in the range $20 \ldots 30\mu$K.

Because of these uncertainties we conclude that the analysis in [22] does not rule out a toroidal universe.

4. Probabilities from the covariance matrix

In [25] the covariance matrix $C_{lm}^{l'm'} := \langle a_{lm} a^{\star}_{l'm'} \rangle$ for the torus universe is compared with the WMAP data and a 95% confidence limit is found that the torus length is $L > 4$. (Here $\langle \ldots \rangle$ denotes an ensemble average.) The covariance matrix for the infinite model $C_{lm}^{l'm'} = C_l \delta_{ll'} \delta_{mm'}$ being diagonal contrasts to the corresponding one of an anisotropic multiply connected space having non-vanishing non-diagonal elements. These can thus serve as a fingerprint for an anisotropic topology of the universe. However, this statement refers to the ensemble average. For an individual model non-diagonal elements are observed in both cases. In Fig. 7 the average $\Sigma := \left\langle \left| \left\langle C_{lm}^{l'm'} \right\rangle_N \right| \right\rangle_{(lm)\neq(l'm')}$ over N models of the non-diagonal elements is shown for several torus models and the infinite ΛCDM model. The grey band shows the average deviation from the mean value for the simulations belonging to the $L = 3.86$ torus. Here and in the following, the covariance matrix is truncated at $l_{\max} = 30$. Numerical tests based on sky maps of the torus model show that for side lengths around $L \simeq 4$ the modes above $l \simeq 20$ do not improve the likelihood to detect a torus topology. Therefore, the restriction to $l \leq 30$ in the covariance matrix is justified. For the infinite model, the average decays as $1/\sqrt{N}$ leading asymptotically to vanishing non-diagonal elements. Fig. 7 shows that the torus models display indeed a deviation from the $1/\sqrt{N}$ decay leading to non-vanishing non-diagonal elements in the covariance matrix. To reveal this behaviour, an average over a large number of models is necessary, but we have observations only from one Universe. In addition, this is aggravated by the large average deviation as shown in Fig. 7. A closer inspection reveals that the non-vanishing non-diagonal elements in the case of the torus models are due to their real parts, whereas the imaginary parts vanish according to the $1/\sqrt{N}$ decay.

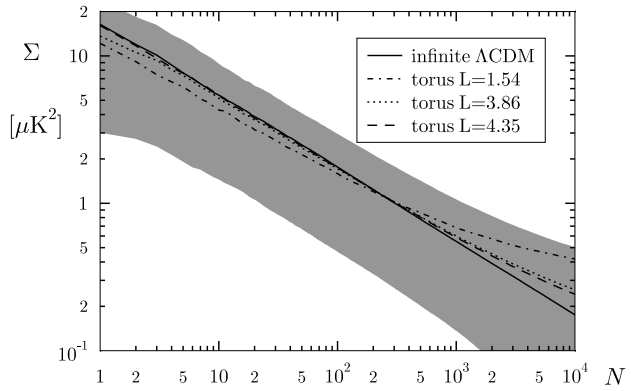

Figure 7. The average Σ of the non-diagonal elements is shown in dependence on the ensemble size N for which the average is computed. The grey band displays the average deviation for the $L = 3.86$ torus ensemble. The $1/\sqrt{N}$ decay in the case of the infinite ΛCDM model is in this logarithmic plot revealed by the straight line with slope $-1/2$. The finite models deviate the stronger the smaller the torus length is in order to approach non-vanishing diagonal elements.

The covariance matrix can nevertheless be used to detect an anisotropic topology by computing the logarithm of the likelihood $\ln \mathcal{L} = -\frac{1}{2}(\ln \det C_{ss'} + \chi^2) + \text{const.}$, where $s := l(l+1) + m$ and $\chi^2 = \min \sum_{s,s'} a_s^\star C_{ss'}^{-1} a_{s'}$. The minimum is obtained by evaluating the sum $\sum_{s,s'}$ for all rotations of a_s, i. e. for all possible orientations of the fundamental cell with respect to the CMB sky. The method of detecting a toroidal universe in this way is discussed in [26, 27]. In Fig. 8 we show $\ln \mathcal{L}$ for the covariance matrix of the torus model in dependence on the length L computed from three different sets of $a_{lm} \equiv a_s$. One set $\{a_s\}$ is computed using a torus model with $L = 3.86$ (full curve) and provides the largest likelihood for the covariance matrix at $L = 3.86$ thus revealing the topology. No such maximum is observed using the a_s obtained from the WMAP-ILC 3yr sky map (without mask) as shown by the dashed curve. Does this exclude a toroidal topology around $L \simeq 4$? The answer depends on the accuracy of the a_s obtained from the WMAP data. This accuracy in turn is determined by the accuracy of the ILC sky map, which we have discussed in the last section. To illustrate this point, we modify the phases of the a_s of the torus model with $L = 3.86$ by $a_s \to a_s \cdot e^{\mathrm{i}r_s}$, where r_s is a Gaussian random variable with unit variance. This blurs the phases by $\simeq 57°$. The result is shown as the dotted curve in Fig. 8 and it is seen that this inaccuracy in the phases destroys the peak at $L = 3.86$. Such an inaccuracy in the phases would make the detection of an anisotropic topology impossible. The accuracy of the phases is discussed in [34, 35] and the WMAP team itself warns of using the ILC map for such a cosmological analysis. In [34] it is shown that the Minimal Variance Method used in the construction of the ILC map leads to a wrong sign for $\sim 40\%$ of the coefficients a_{20} from 10^4 Monte Carlo simulations, i. e. a phase shift of 180°. The assumption that the CMB is a Gaussian random field leads to phases which are uniformly distributed over the interval $[0°, 360°]$. In [35] it is shown that the phases for $l \leq 10$ are consistent with a uniform distribution but not the differences between the phases which should also be uniformly distributed. This should be taken as a warning that the phases might not be sufficiently accurately determined by the ILC map.

Since the accuracy of the phases is unknown, we try to obtain an order of magnitude estimate by the following procedure. Assuming that the ILC map displays outside the kp0 mask the genuine CMB signal, i. e. without any foregrounds, which is surely not true, and within the kp0 mask a strongly disturbed signal which eradicates the CMB signal, we construct sky maps which have outside the kp0 mask the corresponding part of a torus simulation and within the mask a map obtained from an infinite ΛCDM simulation. In this way we combine 950 torus sky maps with 100 infinite ΛCDM sky maps leading to 95 000 data sets of the spherical expansion coefficients a_{lm}. Comparing the phases of these sky maps with the phases of the corresponding torus simulations without mask reveals that the phase change $\Delta\phi$ has a standard deviation $\sigma(\Delta\phi) \simeq 63°$. The large deviations which are of the same order as used in Fig. 8, have their roots in the strong oscillatory nature of the spherical harmonics which leads to many cancellations in the integration required for the computation of the a_{lm}'s. In Fig. 9a the distributions of the phase changes $\Delta\phi$ are shown for four different values of l, i. e. $l = 5$, 10, 20, and 30.

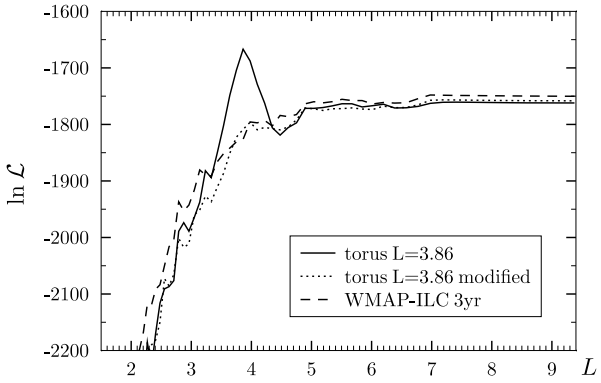

Figure 8. The logarithm of the likelihood $\ln \mathcal{L}$ is shown for the covariance matrix $C_{ss'}$ belonging to the torus model with length L. The χ^2 is computed using the a_s belonging to the torus model with $L = 3.86$ (full curve) and for the a_s obtained from the WMAP-ILC 3yr map (dashed curve). The sharp maximum in the full curve clearly "detects" the underlying torus model. However, modifying the phases destroys the maximum (dotted curve).

The distributions are very similar and have a standard deviation $\sigma(\Delta\phi)$ independent of l as revealed by Fig. 9b. This demonstrates that the accuracy of the phases might be low enough to hide a signature of the topology.

Since the true accuracy of the phases is unknown, one cannot draw a final conclusion whether the covariance matrix signature already rejects a toroidal topology for the Universe. Notice that the correlation function $C(\vartheta)$ and the angular power spectrum δT_l^2 do not depend on these phases such that the very low power at angles $\vartheta \gtrsim 60^\circ$ is a much more robust observation pointing to a non-trivial topology.

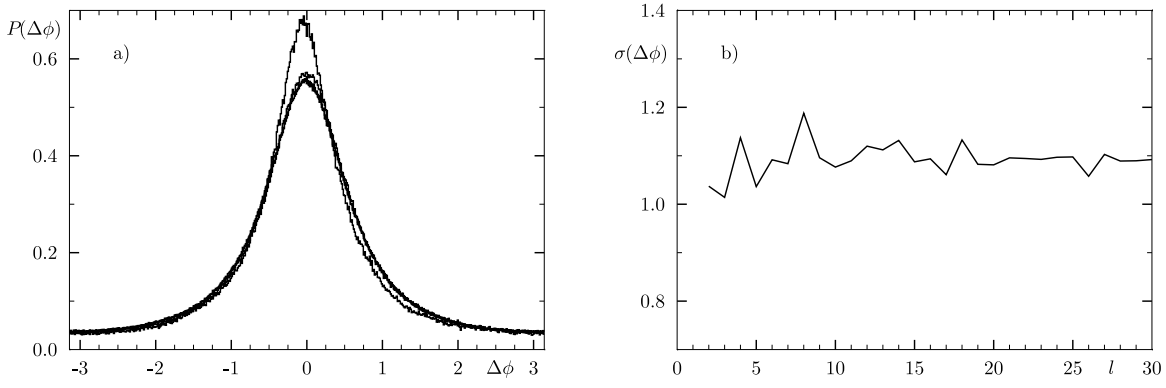

Figure 9. Panel a) shows the distribution of the error $\Delta\phi$ of the phases (in radian) by replacing the torus temperature fluctuations within the kp0 mask by those of an infinite ΛCDM model for $l = 5$, 10, 20, and 30. The distribution with the highest peak at $\Delta\phi = 0$ belongs to $l = 5$ whereas the other distributions are indistinguishable. Panel b) shows that the standard deviation $\sigma(\Delta\phi)$ is $\sigma(\Delta\phi) \simeq 1.1$ independent of l.

The signature of the non-diagonal elements of the covariance matrix $C_{lm}^{l'm'}$ is not only revealed in the spherical harmonics basis but also directly in the pixel space $C(\hat{n}, \hat{n}')$. This alternative is introduced in [36] and applied to compact hyperbolic spaces. In [37] a Bayesian analysis is carried out for the torus model using the pixel space correlation $C(\hat{n}, \hat{n}')$ based on the COBE-DMR data. It is found that for $\varepsilon = L/(2\Delta\eta) \geq 0.6$, i. e. $L \geq 4$, the torus models are consistent with the standard ΛCDM model at the 2σ level, and for some limited choices of orientations the fit to the COBE data is considerably better than that of the infinite model. Such a Bayesian analysis based on $C(\hat{n}, \hat{n}')$ using the WMAP 3yr data is not carried out in this paper such that the advantage of the torus model over the ΛCDM model with respect to this measure remains open here.

5. Summary

Our analysis shows that the simplest non-trivial flat topology, the cubic torus with a side length smaller than the diameter of the decoupling surface, is compatible with the WMAP 3-year data, and describes these data much better than the standard ΛCDM model. It is very intriguing that the toroidal topology provides also the simplest way to solve the problem of initial conditions for the low-scale inflation [29].

CMBFAST (www.cmbfast.org) and HEALPix (healpix.jpl.nasa.gov) [38] were used in this work.

References

[1] D. N. Spergel *et al.*, Astrophys. J. Supp. **170**, 377 (2007), arXiv:astro-ph/0603449.
[2] J. Luminet, J. R. Weeks, A. Riazuelo, R. Lehoucq, and J. Uzan, Nature **425**, 593 (2003).
[3] R. Aurich, S. Lustig, and F. Steiner, Class. Quant. Grav. **22**, 2061 (2005), astro-ph/0412569.
[4] R. Aurich, S. Lustig, and F. Steiner, Class. Quant. Grav. **22**, 3443 (2005), astro-ph/0504656.
[5] R. Aurich and F. Steiner, Mon. Not. R. Astron. Soc. **323**, 1016 (2001), astro-ph/0007264.
[6] R. Aurich, S. Lustig, F. Steiner, and H. Then, Class. Quant. Grav. **21**, 4901 (2004), astro-ph/0403597.
[7] R. Aurich, S. Lustig, F. Steiner, and H. Then, Phys. Rev. Lett. **94**, 021301 (2005), astro-ph/0412407.
[8] K. Schwarzschild, Vierteljahrsschrift der Astron. Gesellschaft **35**, 337 (1900).
[9] Y. B. Zel'dovich, Comments on Astrophysics and Space Physics **5**, 169 (1973).
[10] L.-Z. Fang and H. Sato, Commun. Theor. Phys. **2**, 1055 (1983).
[11] G. F. R. Ellis and G. Schreiber, Phys. Lett. A **115**, 97 (1986).
[12] L. Z. Fang and H. J. Mo, Topology of the universe, in *Observational Cosmology*, edited by A. Hewitt, G. Burbidge, and L. Z. Fang, , IAU Symposium Vol. 124, pp. 461–475, 1987.
[13] I. Y. Sokolov, JETP Letters **57**, 617 (1993).
[14] A. A. Starobinsky, JETP Letters **57**, 622 (1993).
[15] D. Stevens, D. Scott, and J. Silk, Phys. Rev. Lett. **71**, 20 (1993).
[16] Y.-P. Jing and L.-Z. Fang, Phys. Rev. Lett. **73**, 1882 (1994), arXiv:astro-ph/9409072.
[17] A. de Oliveira-Costa and G. F. Smoot, Astrophys. J. **448**, 477 (1995).
[18] A. de Oliveira-Costa, G. F. Smoot, and A. A. Starobinsky, Astrophys. J. **468**, 457 (1996).
[19] J. Levin, E. Scannapieco, and J. Silk, Phys. Rev. D **58**, 103516 (1998).
[20] E. Scannapieco, J. Levin, and J. Silk, Mon. Not. R. Astron. Soc. **303**, 797 (1999), arXiv:astro-ph/9811226.

[21] K. T. Inoue, Class. Quant. Grav. **18**, 1967 (2001), arXiv:astro-ph/0011462.
[22] N. J. Cornish, D. N. Spergel, G. D. Starkman, and E. Komatsu, Phys. Rev. Lett. **92**, 201302 (2004), astro-ph/0310233.
[23] A. Riazuelo, J. Uzan, R. Lehoucq, and J. Weeks, Phys. Rev. D **69**, 103514 (2004), astro-ph/0212223.
[24] A. Riazuelo, J. Weeks, J.-P. Uzan, R. Lehoucq, and J.-P. Luminet, Phys. Rev. D **69**, 103518 (2004), arXiv:astro-ph/0311314.
[25] N. G. Phillips and A. Kogut, Astrophys. J. **645**, 820 (2006), arXiv:astro-ph/0404400.
[26] M. Kunz *et al.*, Phys. Rev. D **73**, 023511 (2006), arXiv:astro-ph/0510164.
[27] M. Kunz, N. Aghanim, A. Riazuelo, and O. Forni, arXiv:astro-ph/0704.3076 (2007).
[28] G. Hinshaw *et al.*, Astrophys. J. Lett. **464**, L25 (1996).
[29] A. Linde, Journal of Cosmology and Astro-Particle Physics **10**, 4 (2004), arXiv:hep-th/0408164.
[30] S. Seager, D. D. Sasselov, and D. Scott, Astrophys. J. Lett. **523**, L1 (1999).
[31] M. Tegmark, A. de Oliveira-Costa, and A. J. S. Hamilton, Phys. Rev. D **68**, 123523 (2003), astro-ph/0302496.
[32] N. J. Cornish, D. N. Spergel, and G. D. Starkman, Class. Quant. Grav. **15**, 2657 (1998).
[33] G. Hinshaw *et al.*, Astrophys. J. Supp. **170**, 288 (2007), astro-ph/0603451.
[34] P. D. Naselsky, O. V. Verkhodanov, and M. T. B. Nielsen, (2007), arXiv:astro-ph/0707.1484.
[35] L.-Y. Chiang, P. D. Naselsky, and P. Coles, Astrophys. J. **664**, 8 (2007), arXiv:astro-ph/0603662.
[36] J. R. Bond, D. Pogosyan, and T. Souradeep, Phys. Rev. D **62**, 043006 (2000), astro-ph/9912144.
[37] K. T. Inoue and N. Sugiyama, Phys. Rev. D **67**, 043003 (2003), astro-ph/0205394.
[38] K. M. Górski *et al.*, Astrophys. J. **622**, 759 (2005), HEALPix web-site: http://healpix.jpl.nasa.gov/.